METAL TO COMPOSITE: REDESIGN OF CENTRIFUGAL PUMP IMPELLER

M. M. N. Frøjk, N. F. H. Bjergmark, R. L. Bjerg, R. Gomila, P. Valero

Department of Materials and Production, Aalborg University
Fibigerstraede 16, DK-9220 Aalborg East, Denmark
Email: mfrajk17, nbjerg17, rpeder16, rgomil20, pvaler20@student.aau.dk,
Web page: http://www.mechman.mp.aau.dk/

Abstract

This article aims to redesign the impeller of the NB 65-200/219 pump from Grundfos, with the objective to reduce the energy consumption when the impeller is accelerated. This is done by changing the impeller's material and optimizing its shape, thereby reducing its weight and mass moment of inertia. The original impeller geometry must be altered without affecting the fluid dynamics inside the impeller. In addition, it is bounded to fit inside the original housing as well as the shaft connection and seals.
To estimate the stresses and life of the original impeller, a Computational Fluid Dynamic (CFD) analysis is coupled one-way with a Finite Element Analysis (FEA).
Regarding the composite alternative, a glass fiber reinforced polyamide (PA66) is selected for redesign which will be manufactured using injection moulding.
A simulation of the injection moulding process is done, exporting the results for fiber orientation and length to a structural analysis done with FEM.
The same process is used to analyse the optimized impeller, which is obtained using a structural shape optimization of the 2D cross section. A sequential quadratic programming is used to reduce the impeller's mass moment of inertia, while constraining the maximum allowed stress and deformation within predetermined limits. The optimized 2D geometry is converted to a 3D model and the structural analysis is run. The results show that this design could replace the original impeller, while reducing the energy consumption of the pump ensuring the same performance.

Keywords: CFD, Composite, FEA, Impeller, Structural Optimisation, Fiber Orientation, Injection Moulding

Detailed descriptions of content within this article, is found in the attached appendix report.

1. Introduction

The focus of this article has been to replace the cast iron NB 65-200/219 Grundfos pump impeller, Figure 1, with fiber reinforced polymer. The motivation behind this replacement is to decrease the pump's energy consumption during startup, which is done by reducing the impeller's mass moment of inertia. In addition, some beneficial properties can be obtained regarding cavitation and resistance to corrosion by changing to a composite material [1].

The fluid dynamics of the impeller will not be changed, as it is assumed to be at an optimum. The inner surfaces of the impeller will therefore be a constraint in the redesign process. This, along with the rest of the impeller's parts can be seen in Figure 2.

A simulation of the impeller's injection moulding process is done, obtaining the fiber orientation and its length. These results are taken into account to calculate the material properties, which are used for the shape optimization of the impeller.

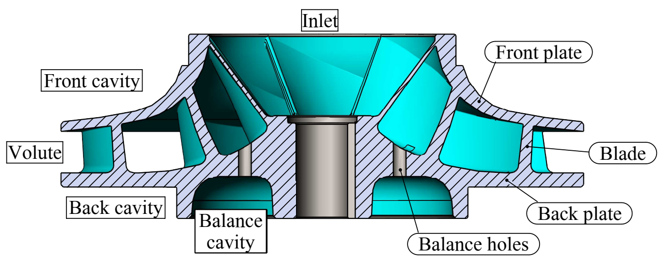

Fig. 2 Cross section of the NB 65-200/219 impeller.

Therefore, the following problem formulation arose:

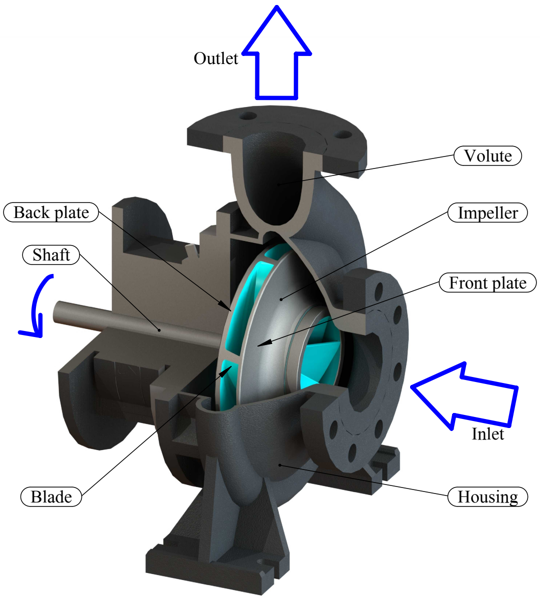

Fig. 1 Centrifugal pump overview.

> *"How can the material of the impeller be switched to a composite material and the impeller optimized with respect to mass moment of inertia, without compromising the mechanical properties?"*

2. Material and Methods

Reducing the impeller's moment of inertia requires different analyses, which are outlined in Figure 3. The pressures acting on the impeller are obtained using Computational Fluid Dynamics (CFD). The resulting pressures are used to run a structural analysis using Finite Element Method (FEM), assessing the mechanical properties of the original impeller.

To redesign the impeller, the manufacturing method and the materials are selected. Afterwards, the manufacturing process is simulated, to obtain the fiber's orientation and length. These will then be used to set up the macro mechanical properties of the impeller for in the FE model.

Based on restrictions from the initial Finite Element Analysis (FEA), a structural shape optimization is used to modify the shape of a 2D cross section of the impeller. Using the results from the optimization a 3D model is created. The orientation and length of the fibers are obtained for the 3D model, which are used to set up the final FE model. The results from the last FEA are compared to those of the original impeller.

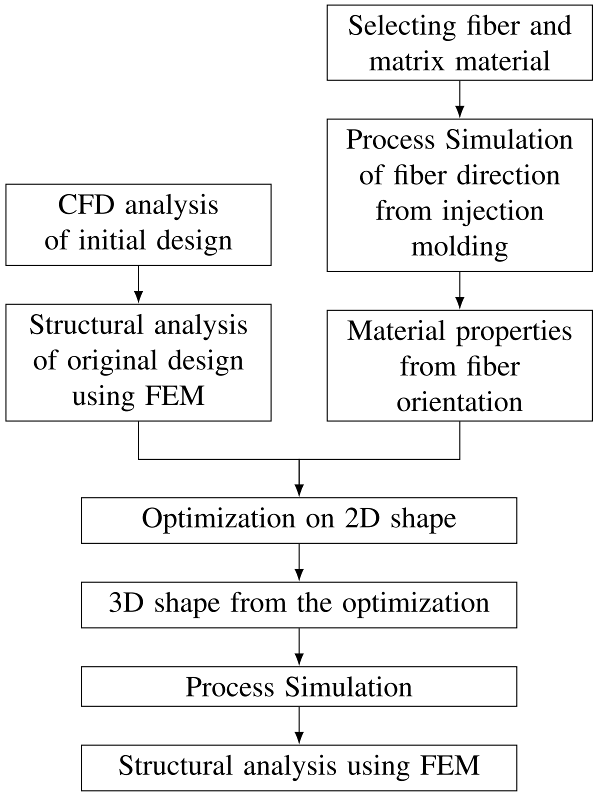

Fig. 3 Flow chart of different methods and analyses used to reduce the moment of inertia.

2.1 Manufacturing technique and material selection

The material selected for the further analyses is **Zytel® 70G30HSLR NC010**, from DuPont [2]. The material is a 30 wt.% glass fiber reinforced polyamide 66 (PA 66). The manufacturing technique to produce the impeller will be injection moulding. The fiber length for the manufacturing analyses is assumed to be 3.4 mm after the screw of the injection unit.

2.2 Injection moulding simulation

A simulation of the flow during the injection process is used to predict the fiber orientation in the moulded impeller. Furthermore, the average fiber length at the end of the injection moulding is also predicted. The effects of the number of gates, gate placement and runner system will be studied. This will be done to achieve a desired fiber orientation in the impeller.

During injection moulding the fibers tend to align with the flow direction along the surfaces, and gradually changing to be transverse to the flow direction in the middle, as shown in Figure 4. This behavior can be used to align the fibers with the maximum principal stress, utilizing the strength and stiffness of the fibers.

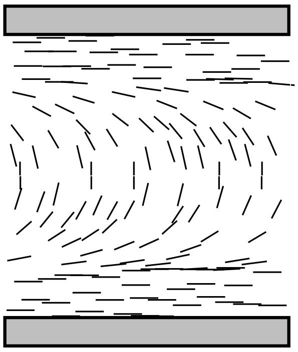

Fig. 4 Visual representation of fiber orientation through the thickness.[3]

2.3 Material modeling

The program Digimat is used to obtain a FE model that takes the fiber orientation and the fiber lengths into account to calculate the macro mechanical properties. Digimat uses a two-step homogenization process as shown in Figure 5. The real composite representative volume element (RVE) is replaced with a RVE made out of *pseudo-grains*, Figure 5(a). Each of these pseudo-grains is a two-phase composite that has a phase of inclusions aligned over one small range of orientations and a bonding matrix. The next step consists of homogenizing each pseudo-grains separately, using the Mori-Tanaka mean-field homogenization, Figure 5(b). The final step uses the Voigt model to completely homogenize all the pseudo-grains into one RVE, Figure 5(c). [4]. Digimat will also be used to set up static- and fatigue failure index with dependence on the fiber orientation.

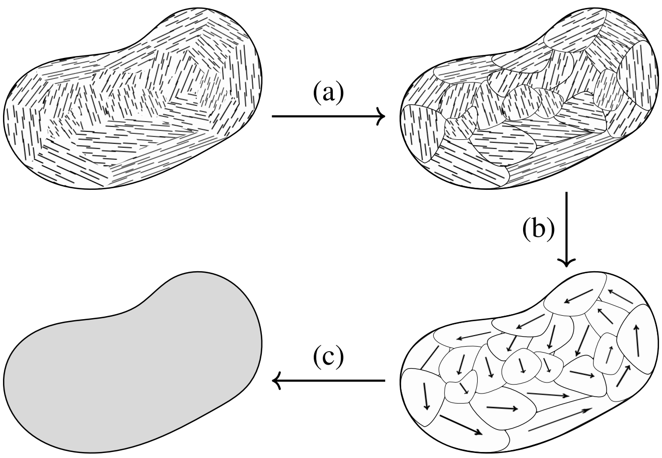

Fig. 5 Digimat two-step homogenization.

2.4 Fiber Composite Failure Criterion

The 3D *Tsai-Hill transversely isotropic strains based failure criteria* has been used to assess the strength of the composite impeller. The criteria presented in Equation 1 is taken from [4]. The maximum strains at failure, used to define the criteria, were available in Digimat for the material chosen and are presented in Table I. The assumption of transverse isotropy is in general not true for the injection moulded impeller however at surfaces where the stresses are higher. Thus, where the failure is expected to occur, the fibers are oriented in a preferable direction. In these regions this assumption is considered valid.

$$
\begin{aligned}
F_A(\varepsilon) = {} & \frac{\varepsilon_{11}^2}{X^2} - \frac{\varepsilon_{11}(\varepsilon_{22}+\varepsilon_{33})}{X^2} + \frac{\varepsilon_{22}^2+\varepsilon_{33}^2}{Y^2} \\
& + (\frac{1}{X^2} - \frac{2}{Y^2})\varepsilon_{22}\cdot\varepsilon_{33} + \frac{(2\varepsilon_{12})^2+(2\varepsilon_{13})^2}{S^2} \\
& + (\frac{1}{Y^2} - \frac{1}{4X^2})(2\varepsilon_{23})^2
\end{aligned}
\tag{1}
$$

	Strain at failure
Maximum axial tensile strain X	0.03722
Maximum in-plane tensile strain Y	0.04414
Maximum transverse shear strain S	0.10556

Tab. I Maximum strains at failure

The fatigue failure criteria used for the fiber composites is also the Tsai-Hill 3D transversely isotropic. The same assumption regarding the fiber orientation is made as before. This criteria is capable of capturing the effects of the material's anisotropy as well as the mean stress influence. In this criteria the material's strength parameters for the static failure are substituted by the stress amplitudes at failure (fatigue strengths) for a determined number of cycles. The S-N curves, both for the axial tensile loading and transverse tensile loading of an unidirectional specimen with a fatigue ratio $R = 0.1$, have been obtained from [5]. In the article, the same material as the one selected for the impeller is used. The shear loading S-N curve has been assumed to be the same as the transverse loading due to limited data available. The constant life diagrams (CLD) presented in [6] were used. The material in the article does not have the same fiber weight fraction as selected for the impeller, therefore, small adjustments are done to the CLD.

2.5 CFD

Data from the pump operation at its maximum flow rate, $Q = 80\,\mathrm{m^3\,h^{-1}}$, is used for the CFD analysis to determine the load case for the impeller i.e. the pressures acting on the impeller. The CFD analysis is a dynamic analysis that uses implicit time integration for solving the Naiver-Stokes equations for a finite volume along with continuity equations.

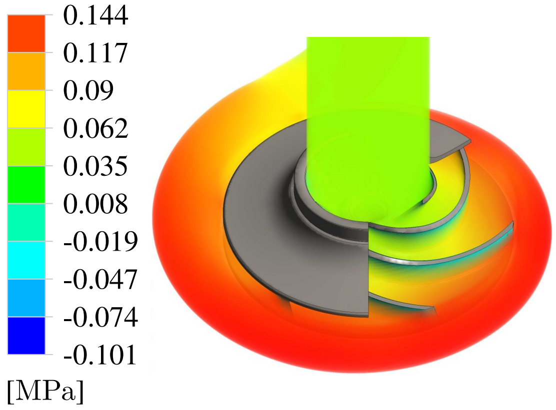

Fig. 6 CFD pressure results

2.6 FEM

The deformation, stresses and strains in the impeller are determined with a linear static structural analysis using FEM. This method calculates the displacement of a model discretized into a mesh of elements by solving the linear system of equations shown in Equation 2, where $[K]$ is the global stiffness matrix, $\{D\}$ is the global displacement vector and $\{R\}$ is the global load vector. After solving this system of equations, strains and stresses can be calculated.

$$[K]\{D\} = \{R\} \tag{2}$$

The results from the FEA are used as a starting point for the redesign.

The maximum deformation value is equal to 8.35×10^{-3}mm. It is located on the front plate, precisely on the cavity closer to the outlet, where the pressure inside the impeller is lower. The maximum von Mises stress is equal to $60.86\,\mathrm{MPa}$ and it is located on the fillet of the corner, closer to the maximum deformation where the blade joins the front plate, as shown in Figure 7.

2.7 Optimization

Due to the complexity and computational cost of shape optimization, the FEA of the impeller is simplified to a 2D model. This model is a compromise between accuracy and computational efficiency.

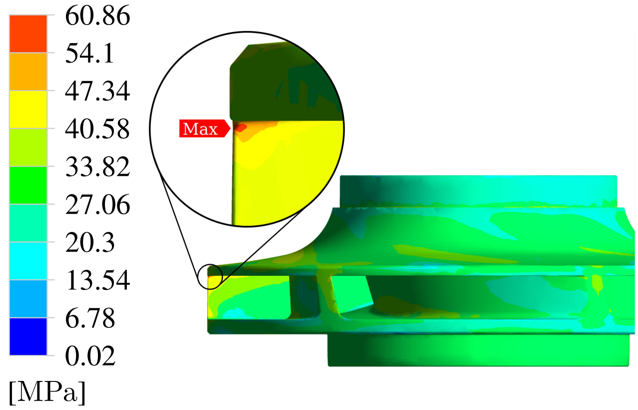

Fig. 7 Von Mises stress on the impeller

The impeller is converted to a 2D axis-symmetric model where this axis symmetry introduces an automatic boundary condition to the 2D model. Thus, the elements cannot displace in the radial direction without straining in the tangential direction.

The objective of the optimization is to minimize the mass moment of inertia of the impeller to be less than the original $22.4 \cdot 10^{-3}\,\mathrm{kg\,m^2}$.

To state the general constraints for the optimization, a maximum allowable stress and deformation is evaluated. As the stress concentration in the fillet at the edge of the impeller cannot be approximated with the 2D model, some predictions are made. The maximum von Mises stress in the 2D model is associated with the maximum von Mises stress in the 3D model. This is done via linear extrapolation. Thus, the relation between the two is approximated to a factor of 10. From this assumption the max allowable stress in the 2D model, is found to be $5.0\,\mathrm{MPa}$.

For the deformation, roughly $70\,\%$ of the total deformation is in the tangential and thus out of plane direction. This allows the 2D model to deform only $30\,\%$ of the total deformation restriction at $0.2\,\mathrm{mm}$.

The impeller is given some keypoints, which are defined by a location and a design variable (DV) with one degree of freedom.

This allows the optimization algorithm to change the DV position and thus the geometry of the model. The DV movement is bound by a set of restrictions, chosen to be at the limit of minimum wall thickness in the injection moulding process, and so the impeller will still fit within the pump housing. The keypoints and the bounds are illustrated in figure Figure 8.

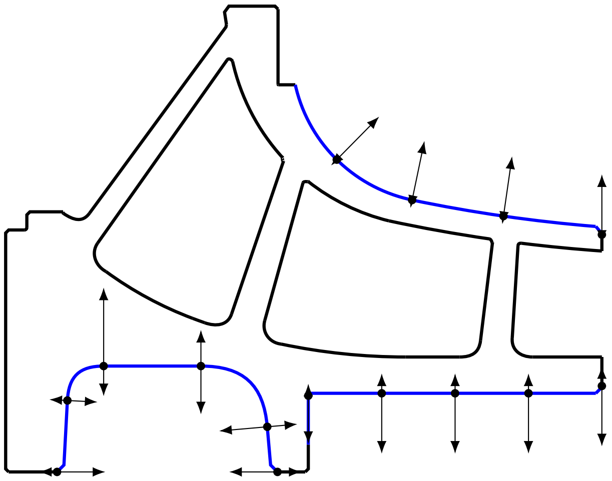

Fig. 8 Bounds for the design variables used for the shape optimization of the 2D model.

3. Results

3.1 Process Simulation

The injection moulding process is simulated. The runner system is designed locating six gates on the front plate at the end of the blades, as seen in Figure 9. This is done to achieve the melt flow along each one of the blades, orienting the fibers throughout the process.

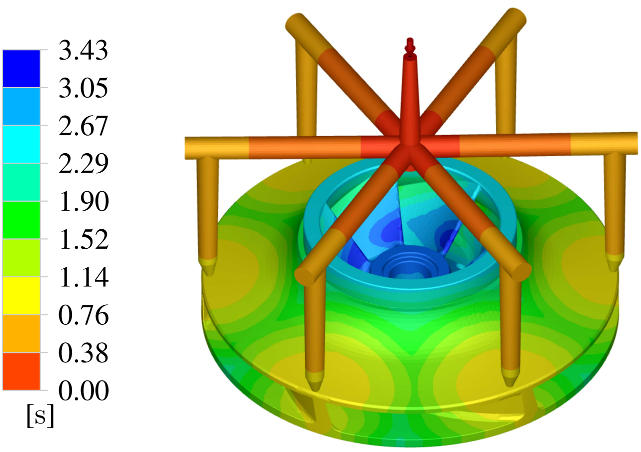

Fig. 9 Runner system setup and melt front advance.

In Figure 10 the first eigenvector of the orientation tensor can be seen at the end of the filling process. The eigenvector shows the orientation with its magnitude (eigenvalue) describing the degree of orientation. Random orientation would have a value of 0.33 and the closer it approaches 1, the higher the fiber alignment. Thus, as introduced in Figure 4, a random orientation is exhibited at the center, while closer to the surface the fibers are highly oriented with the flow direction.

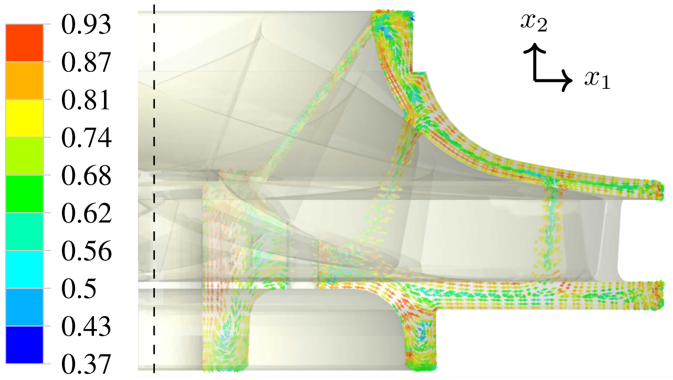

Fig. 10 First eigenvector of the fiber orientation tensor and its magnitude.

In addition, the fiber breakage during the injection moulding is calculated. From the original fiber length at the sprue of $3.4\,\mathrm{mm}$, the resulting average fiber length, measured by weight, is obtained with a value $1.640{\pm}0.270\,\mathrm{mm}$. The fiber orientation tensor as well as the average fiber length is exported to set up the static analysis.

3.2 Optimization results

The final result of the optimization is shown in Figure 11. The algorithm has removed material in most parts of the impeller. The von Mises stress is also shown in the Figure 11, where it is generally higher in the optimized impeller.

The results of the optimization is shown in Table II, from which the mass moment of inertia is concluded to have a reduction of $-86.5\,\%$ after the material change and optimization. Moreover, the maximum von Mises (vM) stress does not experience a significant change.

	Mass [kg]	Moment of Inertia $[10^{-3}\,\mathrm{kg\,m^2}]$	Max. VM stress [MPa]	Max. Deflection [mm]
Original	4.51	22.4	60.86	0.008
Optimized	0.62	3.03	63.03	0.271
Change	$-86.3\,\%$	$-86.5\,\%$	$3.6\,\%$	$3146\,\%$

Tab. II Results

The largest total deformation, with a value of $0.271\,\mathrm{mm}$ is found on the back plate between two blades, as shown in Figure 12. It is caused by the pressure difference between the outside and inside. The fillet where the blade joins the front plate is where the maximum von Mises stress is found with a value of $63.03\,\mathrm{MPa}$.

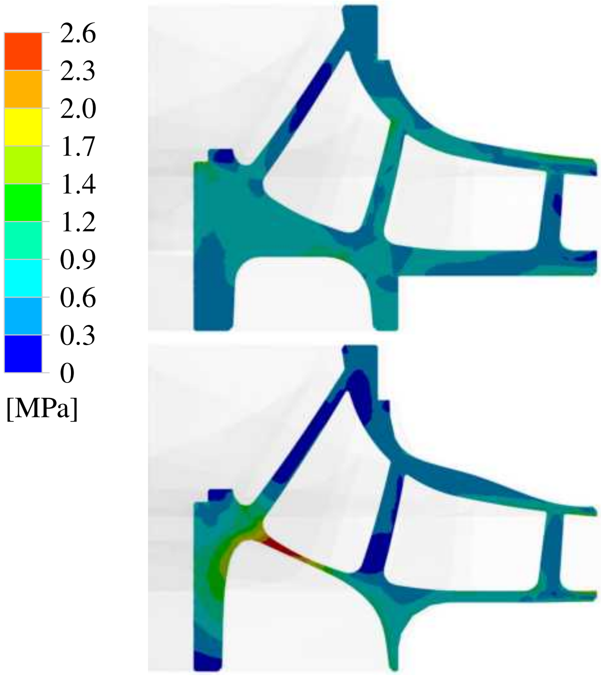

Fig. 11 Comparison of the von Mises stress in a cross section of the original impeller and the optimized impeller.

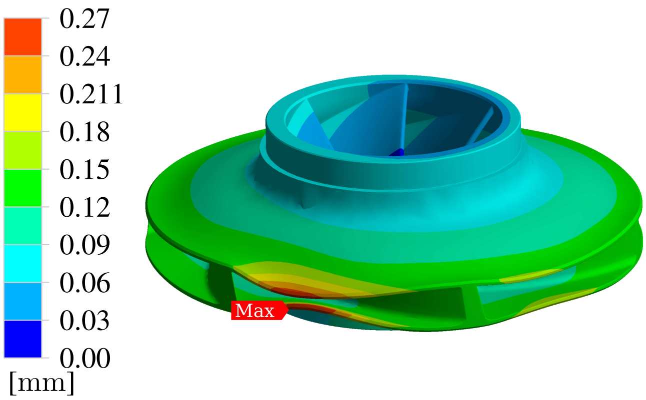

Fig. 12 Total deformation of the optimized impeller

In Figure 13, the indicator of alignment between the stress tensor and the fiber orientation tensor is presented. It can be seen that a good alignment has been achieved on the front and back plate, where the highest stresses are located.

Using the SN-curves and constant life diagrams the fatigue failure indexes for the optimized composite impeller are calculated. The results for the indexes are shown in Table III, for both the worst case where the largest stress is transverse to the fiber orientation, and the best case where they are aligned.

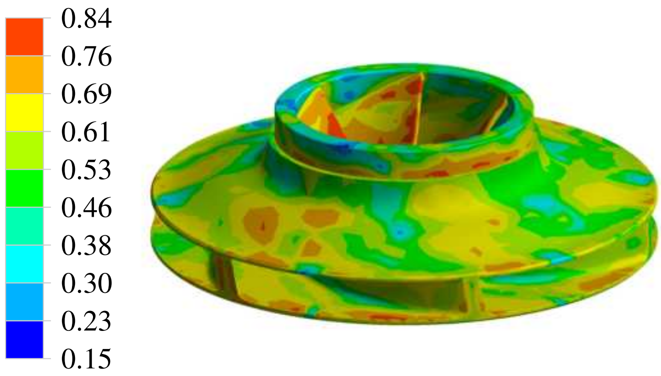

Fig. 13 Alignment of the stresses and fiber orientation

Cycles	Non-aligned stress	Aligned stress
10^9	1.13	0.51
10^{10}	2.38	0.66

Tab. III Fatigue failure indexes

4. Discussion
4.1 Optimization

During the initial run, the balancing cavity was the less altered zone as the keypoints here have a smaller influence on the moment of inertia. This is due to the fact that it is a cross section of an axis symmetric object, meaning that the distance from the center makes the volume of the element greater. Furthermore, the distance from the center is squared in the calculation of the moment of inertia. Thus the difference between the influence of an element near the center and one at the edge is proportional to the radius cubed.

The optimization was done for a simplified 2D model of the impeller.Out of plane deformations were not taken into account. This resulted in a total deformation in the 3D model larger than the constraint. The equivalent constraint in the 2D model, could be made more conservative to get a better result. However, it was assumed the deformation would not affect the fluid dynamics of the impeller significantly.

Better results could be obtained through a full 3D optimization model. Other simplifications for the structural influence of the blades, the varying anisotropic mechanical properties, and the load case were done to reduce the computational cost of the optimization. All these compromises are potentially deviating the 2D optimum design from the 3D optimum thus a 3D optimization should be done.

4.2 Fiber Alignment and Fatigue

The worst fatigue failure index for the optimized impeller is 2.38 at 10^{10} cycles. However, this failure index is only for the case where the alternating stress is acting in the transverse direction of the fiber orientation. Since the fiber orientation in the fillet is in between aligned and transverse, it is assessed that the impeller will not fail due to fatigue before 10^{10} cycles.

The fatigue failure criteria used in this paper has been the 3D Tsai-Hill transversely isotropic failure criteria. Although this assumption is not valid for the whole domain, it has been the only option available. This is due to the limited empirical data available.An assumption of orthotropy or full anisotropy would be more accurate if enough material data was available. Furthermore, with more material data, it would also be possible to take into account the difference between tension and compression loading, using a different failure criteria like the Tsai-Wu.

A transient analysis of a full rotation of the impeller could be used to do a more accurate fatigue analysis. This could be used to calculate the correct load ratio at each node thus giving an estimate of fatigue life for each node of the model. This could also be used to identify different alternating stresses that have not yet been taken into account.

4.3 Cavity pressure

The leak-flow occurring in the front and back cavities is not included in the CFD model. This means that the CFD does not calculate the pressure on the outside of the impeller. To avoid unrealistic results in the FEA, these pressures are calculated from the velocities inside the impeller. The velocities have been averaged over the impeller interface, resulting in a high pressure zone on the front plate and a low pressure zone inside the channel closest to the outlet. This pressure difference provokes the biggest deformation and highest stresses of the model. Because of this, the critical values used to assess the integrity of the impeller and dimension the redesign, are believed to have a high uncertainty, potentially being higher than the real ones.

4.4 Cavitation

The matrix material selection has been partially based on good properties against wear from cavitation. However, no analysis has been done to try to determine the wear. The best way to assess this is by doing experiments from which the results can be used to dimension the impeller parts more exposed to cavitation.

4.5 Visco elastic properties

The material properties selected were obtained from literature for a temperature of $23\,^{\circ}\mathrm{C}$. However, polymer properties such as stiffness, strength, and fatigue life are highly dependent on the temperature. Grundfos states an operation range from $5\,^{\circ}\mathrm{C}$ to $120\,^{\circ}\mathrm{C}$ thus further analysis with different material properties should be done.

Moreover, creep might be affect the impeller due to the applied torque. Although the material's creep compliance is high in caparison to common polymers, it will still result in a $1\,\%$ strain in the most severe stress concentration over the course of $1000\,\mathrm{h}$.

5. Conclusion

The impeller of the NB 65-200/219 Grundfos pump was redesigned by changing the material from cast iron to glass fiber reinforced polyamide. The shape of the impeller was changed using an optimization algorithm, reducing its mass moment of inertia. The new impeller designed ended up having a mass moment of inertia that was $86.5\,\%$ less than the initial design, while keeping the estimated fatigue life within the preset limit. The new material has some advantageous properties with regard to cavitation and corrosive resistance, which would prolong the impeller's estimated life compared to cast iron. Further work is necessary before the new impeller design is ready for production. However, this paper shows that significant improvements of the mass moment of inertia is obtainable through a redesign of the original impeller using composite materials.

Acknowledgements

The authors of this work gratefully acknowledge Grundfos for sponsoring the 8th MechMan symposium, as well as Therkel Damm for making a collaboration with Grundfos possible.

Furthermore, we would like to acknowledge Mads Jespersen from FlowHow, for providing a Moldex3D educational license.

References

[1] "Composite impellers produce significant life-cycle savings." https://bit.ly/3sFGWc3, 2011.
[2] D. M. D. Center, "Zytel® 70g30hslr nc010." https://bit.ly/33yLPt4, 2021. Accessed: 2021-05-03.
[3] S. G. Advani and K.-T. Hsaio, Manufacturing techniques for polymer matrix composites (PMCs). Cambridge: Woodhead Publishing Ltd, 2012.
[4] e Xstream, "Digimat user's manual," 2021.
[5] Y. Zhou and P. Mallick, "Fatigue performance of an injection-molded short e-glass fiber-reinforced polyamide 6,6. i. effects of orientation, holes, and weld line," Polymer Composites, vol. 27, 04 2006.
[6] M. J. Kanters, L. F. Douven, and P. Savoyat, "Fatigue life prediction of injection moulded short glass fiber reinforced plastics," Procedia Structural Integrity, vol. 19, pp. 698–710, 2019. Fatigue Design 2019, International Conference on Fatigue Design, 8th Edition.